

Silicon Photonics Design, Fabrication and Data Analysis for Mach-Zehnder Interferometers and a Lattice FIR Filter - AllenJustin

AJ

the date of receipt and acceptance should be inserted later

Abstract Parameters and analysis are explored for several Mach-Zehnder Interferometers and one Lattice FIR filter. Detailed design simulations and comparisons with a physical resulting fabricated wafer from University of Washington's nano-fabrication facility are explored.

1 Introduction

A core building block to many Silicon Photonics circuits with a vast variety of applications is a Mach-Zehnder Interferometer (MZI). This building block in the combination with other technologies may be used to create optical communications, switches, adjustable splitters [1], sensors for pressure, flow, aerodynamics [2], and within biological, chemical, and environmental industries[3]. Exploring the physical parameters when designing a MZI enables comprehension into how an MZI is leveraged for these multitude of applications and future possibilities. MZI's may be cascaded into stages to form a lattice Finite Impulse Response (FIR) filter as well and this more advanced application for an MZI will be touched on.

2

3 Theory

The Mach-Zehnder Interferometer (MZI) provides the ability for light in an optical path to be split and travel in two parallel optical paths and then recombined for the output. The theory is if the two parallel optical

paths are of the same length then the output light intensity (I_o) is equal to the input light intensity (I_i) due to constructive interference. If the MZI is "imbalanced" with a differing length between the two parallel optical paths this causes a phase shift which theoretically with a phase difference of π would lead to complete destructive interference and no power on the output. Thus the MZI branches are considered phase shifters that through altering parameters such as physical length. Altering other properties in an MZI branch can change the index of refraction and thus output phase. These include temperature changing the index of refraction via the thermo optical effect or PN diode altering the depletion region above the branch.

For our MZI silicon photonics application we pass light into a y-branch, 2 wave guides, and then recombine it in another opposite facing y branch. The branch intensities can be modeled for constructive interference or light in phase as

$$I_1 = I_i/2$$

$$I_2 = I_i/2$$

$$\text{and thus } I_o = I_i$$

However given $I \propto |E|^2$ we know then the complex electric field in each branch is

$$E_1 = E_i/\sqrt{2}$$

$$E_2 = E_i/\sqrt{2}$$

$$\text{and thus } E_o = \frac{E_1 + E_2}{\sqrt{2}}$$

We can see our outputs will be dependent on the driving variables for the plane wave mainly

$$E = E_o * e^{i(\omega t - \beta z)}$$

where $\beta = \frac{2\pi n}{\lambda}$ where n is the index of refraction. We see that the output varies sinusoidally with respect to the wavelength of the light and the index of refraction as well as time and space. The length of the branches L_1 and L_2 are substituted into the z position variable to find the E_o in the above equations.

$$E_{o1} = \frac{E_i}{\sqrt{2}} e^{-i\beta_1 L_1 - \frac{\alpha \text{Im} \beta_1}{2} L_1} \text{ and } E_{o2} = \frac{E_i}{\sqrt{2}} e^{-i\beta_2 L_2 - \frac{\alpha \text{Im} \beta_2}{2} L_2}$$

Plugging in the above to $I \propto |E|^2$ gives us

$I_o = \left| \frac{E_{o1} + E_{o2}}{\sqrt{2}} \right|^2$ simplifies down to when we consider the lossless case given $\alpha = 1$ and given identical wave guides with the same index of refraction and physical properties in our case then $\beta_1 = \beta_2$ then we can derive an equation for an imbalanced interferometer

$$I_o = \frac{I_i}{2} [1 + \cos(\beta \Delta L)]$$

Here we see our output sinusoidally varies based on wavelength, index of refraction, and length.

3.1 Free Spectral Range (FSR)

When characterizing an interferometer design the Free Spectral Range (FSR) is noted which basically describes the period or distance between two max I_o over varying wavelengths of light. This describes for what bandwidth's and frequencies the output will be passed verses attenuated.

Following derivations given by [1] we are given a term for group index (n_g) related to group velocity based off of effective index (n)

$$n_g = n - \lambda \frac{dn}{d\lambda}$$

$$FSR = \frac{\lambda^2}{\Delta L n_g}$$

3.2 MZI Transfer Function

The transfer function allows us to calculate the output power in dB based on the input power. This function includes the "Waveguide compact model" namely the Taylor series expansion of

$$n_{eff}(\lambda) = n_1 + n_2(\lambda - \lambda_0) + n_3(\lambda - \lambda_0)^2$$

and

$$\beta(\lambda) = \frac{2\pi n_{eff}(\lambda)}{\lambda} + i\frac{\alpha}{2}$$

α is the propagation loss within the waveguide where for this design we assume 3 to 4 dB/cm

$$T_{MZI-dB}(\lambda) = 10 \log_{10} \left(\frac{1}{4} |1 + e^{-i\beta(\lambda)\Delta L}|^2 \right)$$

4 Modelling and Simulation

The designs that will shown to be modeled, simulated, fabricated, and analyzed include 4 MZI circuits for the E field of varying ΔL branches, 1 MZI in the H field, and 1 experimental lattice FIR filter of multiple staged MZI's. All MZI's designed are as shown below with include a gradient coupler for the test laser input, followed by a Y branch, followed by the two imbalanced wave guides which connect to a 50/50 broadband directional coupler (BDC) splitter followed connected by

waveguides to the gradient couplers for reading the outputs. The factors under test discussed below are the waveguide parameters mainly width and their lengths. It was chosen to use BDC instead of just a Y branch on the output to allow for 2 outputs which should be 180 degrees out of phase from each other, often used for switches and similar applications. The layout took care for all E field MZI circuits to keep waveguide bend radius $> 5 \mu\text{m}$ while it is noted the H field MZI should meet the requirement of bend radius $> 10 \mu\text{m}$. This may be discussed further below.

The MZI circuits being designed will be characterized at wavelengths centered around 1550 nm with about 100 nm bandwidth, ranging from 1500 to 1600 nm. This matches the future wafer automated testing that will be performed.

The core wave guide component designed is restricted to 220 nm high and chosen width of 500 nm allows ideal single mode propagation for E field or H field greatly suppressing the higher order modes as will be shown.

4.1 3.1 Waveguide Properties

Our 500 nm wide, 220 nm high waveguides can be shown to have about index of refraction $n_{eff} = 3.47$ for Si and $n_{eff} = 1.44$ for SiO₂ as shown in the below Lumerical Mode analysis setups.

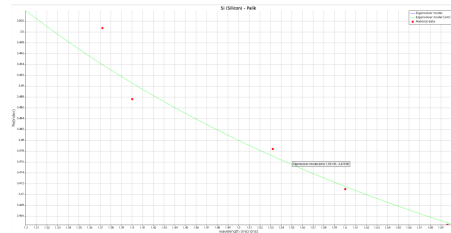


Fig. 1 index of refraction for designed Silicon Waveguide from Lumerical Mode Analysis

Below we can see the intensity of the Efield and the Hfield's in the waveguide using the Lumerical Mode Eigensolver Analysis

Note our intensity is in the horizontal direction for the E field and vertical direction for the H field as expected. If we plot the energy density in linear scale we see the majority of the optical energy remains within the Si waveguide.

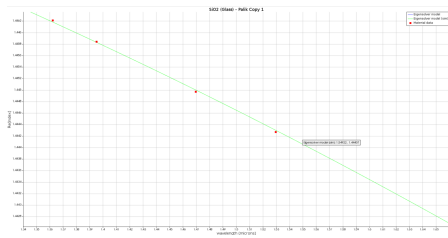


Fig. 2 index of refraction for SiO2 layers around Si waveguide for models done from Lumerical Mode Analysis

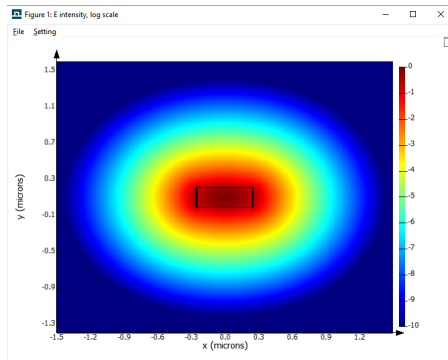


Fig. 3 Efield intensity dB scale within our waveguides

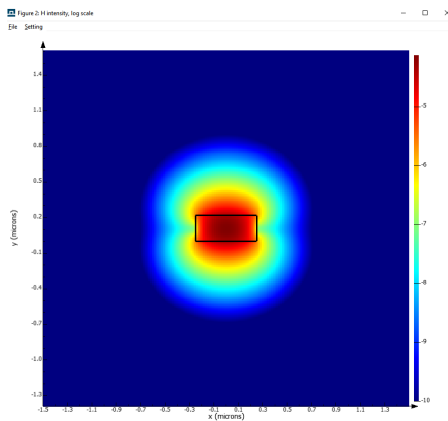


Fig. 4 H field intensity within our waveguide

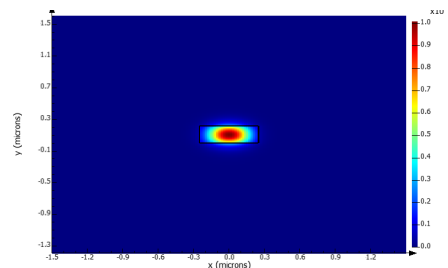


Fig. 5 Energy density within our waveguide

5

Plotting our waveguides effective index and group index over wavelengths

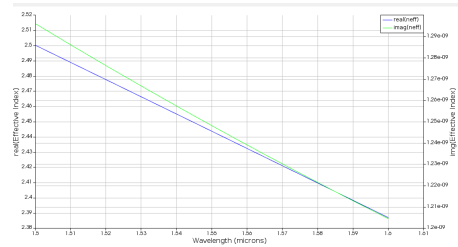


Fig. 6 n_eff for our waveguide about 2.445 at 1550nm

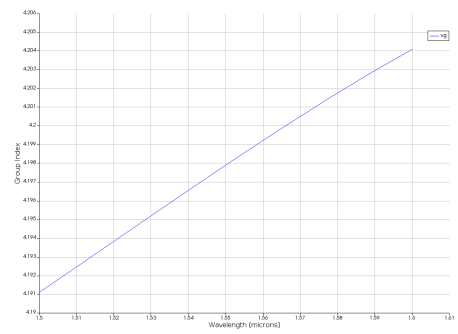


Fig. 7 n_group index for our waveguide about 4.198 at 1550 nm

5.1 Compact Model for our Waveguide

Given the prior information we can come up with a Taylor expansion expression for n_{eff}

$$n_{eff}(\lambda) = n_1 + n_2(\lambda - \lambda_0) + n_3(\lambda - \lambda_0)^2$$

Leveraging [1] matlab code to match our Lumerical Mode generated data to the above expression we calculate the values for $n_1, n_2,$ and n_3 for $\lambda = 1.55$ to be

$$n_{eff}(\lambda) = 2.44365 - 1.13171(\lambda - 1.55) - 0.0424756(\lambda - 1.55)^2$$

6

6.1 Waveguide Properties to Consider

While performing analysis some other relationships to note for an ideal waveguide 500nm x 220 nm at wavelength of 1550 nm include:

- * $n_{eff} = 2.445$: effective index decreases as lambda increases.
- * waveguide loss = 4.39 db/cm : decreases as wavelength increases
- * $n_g = 4.198$: Group index increases with wavelength
- * $v_g = 7.141$ m/s : Group velocity decreases with wavelength
- * $g_{delay} = 1.4$ ps/km : Group delay increases with wavelength
- * Dispersion = 446 ps/nm/km and isn't linearly related
- * Beta = .99 1/m : decreases with wavelength

6.2 Lumerical Simulation Analysis

The below shows lumerical simulation analysis for the below chosen ΔL combinations.

The FSR can be calculated using the above equations or through simulations as shown below.

Cell Name	Field H or E	L1 (um)	L2 (um)	DeltaL (um)	FSR (nm) Simulated
MZI1	E	47.608	74.486	26.878	22.5
MZI2	E	47.608	74.486	26.878	22.5
MZI3	E	47.608	133.535	85.927	7
MZI4	E	53.7428	87.485	33.737	17.5
MZI5	H	41.838	33.338	8.5	80
FIR1	E	n/a	n/a	n/a	filter BW 3dB 50nm?

Notes:
 FSR = $\lambda^2 / (\Delta L \cdot n_g)$
 FSR(nm) Simulation was kicked off directly from the Klayout MZI's connected to Lumerical Interconnect

Fig. 8 Simulation FSR results

MZI4 the “detector2” port is cleanly centered about 1550 nm with 17.5 nm of FSR. This is the select MZI to perform measurements on.

Note as our delta L increases then our FSR decreases.

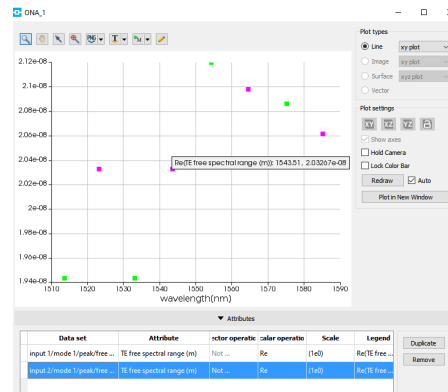


Fig. 9 FSR values for MZI1

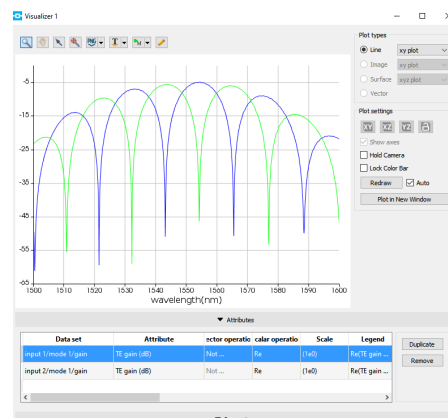


Fig. 10 MZI1 gain: FSR 22.5

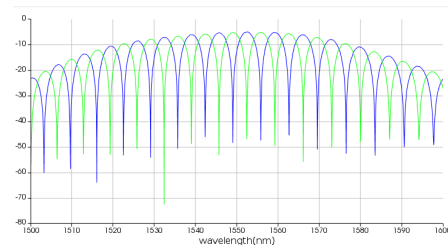


Fig. 11 MZI3 gain: FSR = 7nm

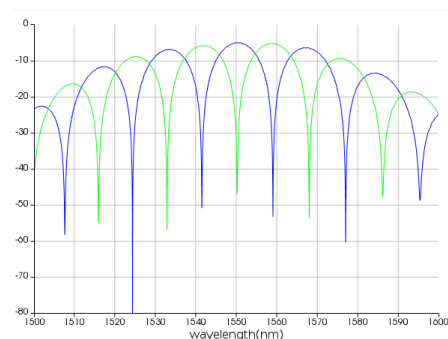


Fig. 12 MZI4: FSR = 17.5 nm

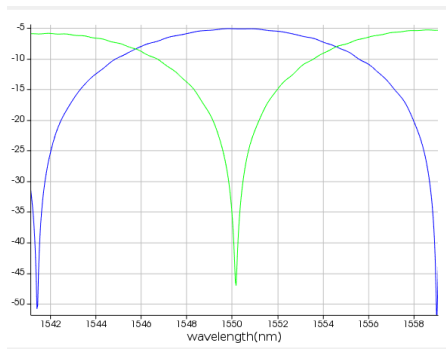


Fig. 13 MZI4: FSR = 17.5

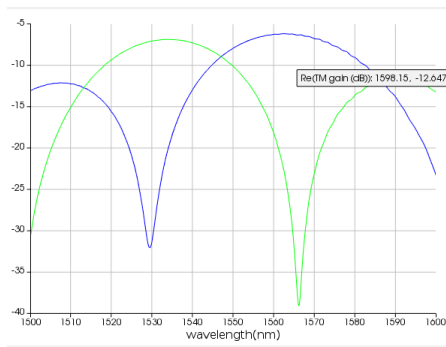


Fig. 14 MZI5: TM polarized with waveguide turns below radial requirement, FSR about 80?

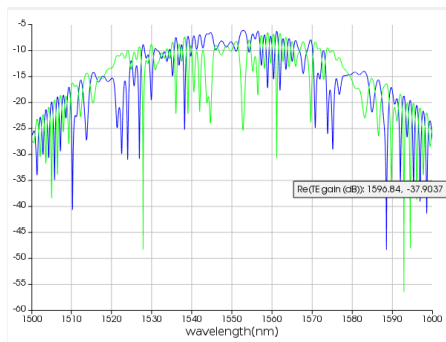


Fig. 15 intended FIR filter, however didnt carefully design or calculate parameters

6.3 Modeling for Fabrication

6.3.1 Waveguide Dimension Variations

The wafer height of 220 nm varies and the waveguide width isn't perfect as well as the rectangular waveguide isn't perfect rectangle with not ideal 90 degree angles but slopes like a trapezoid from base to top. These manufacturing variabilities require analysis with error variance to allow us to know what our expectations are. For the MZI peak wavelength, insertion loss, group

index, FSR and the extinction ratio of the inferometer will all be affected by these manufacturing imperfections.

Corner analysis is performed to refine our MZI behaviour predictions following a process such as [1] description below:

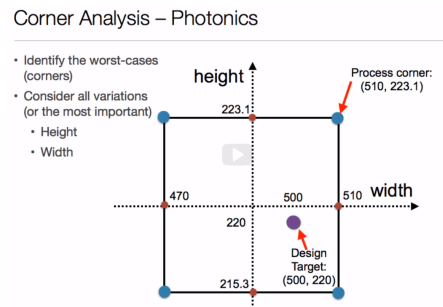


Fig. 16 This is a caption

For our corner analysis case we analyzed for the above range variations to height and width, checking all 4 corners and the ideal case to provide limits.

CORNER	n _g	n _{eff}
Nominal (220 nm x 500 nm)	4.198	2.445
LL (215.3 nm x 470 nm)	4.2444	2.372
UL (223.1 nm x 470 nm)	4.258	2.0438
LR (215.3 nm x 510 nm)	4.1735	2.44
UR (223.1 nm x 510 nm)	4.186	2.475

Fig. 17 Corner Analysis via Lumerical Mode for waveguide fabrication variation

6.3.2 Bandwidth Limited Grating Couplers

Due to bandwidth limited grating couplers with finite bandwidth we must model within our simulations the ideal flat FSR response will rather be attenuated significantly on the order of 10 dB only 20 nm away from the intended center frequency. Since there are manufacturing variations during fabrication as well, we need to simulate and model with these variation thresholds to estimate what our fabricated design results will look like. There is also waveguide propagation loss which can be up to 6.6 dB/cm at 1550 nm.

We can lowpass filter the data and flatten it out for analysis.

Another method to model is to do on chip calibration structures to subtract out the difference.

We can do curve fitting for our model as well, we do this finding peaks or auto correlation to find period of our signal. We can compensate for group index and dispersion in our waveguide. We can then decide if our experimental results match our simulated results.

7 Fabrication

7.1 Washington Nanofabrication Facility (WNF) silicon photonics process:

The devices were fabricated using 100 keV Electron Beam Lithography [[4]]. The fabrication used silicon-on-insulator wafer with 220 nm thick silicon on 3 μm thick silicon dioxide. The substrates were 25 mm squares diced from 150 mm wafers. After a solvent rinse and hot-plate dehydration bake, hydrogen silsesquioxane resist (HSQ, Dow-Corning XP-1541-006) was spin-coated at 4000 rpm, then hotplate baked at 80 $^{\circ}\text{C}$ for 4 minutes. Electron beam lithography was performed using a JEOL JBX-6300FS system operated at 100 keV energy, 8 nA beam current, and 500 μm exposure field size. The machine grid used for shape placement was 1 nm, while the beam stepping grid, the spacing between dwell points during the shape writing, was 6 nm. An exposure dose of 2800 $\mu\text{C}/\text{cm}^2$ was used. The resist was developed by immersion in 25% tetramethylammonium hydroxide for 4 minutes, followed by a flowing deionized water rinse for 60 s, an isopropanol rinse for 10 s, and then blown dry with nitrogen. The silicon was removed from unexposed areas using inductively coupled plasma etching in an Oxford Plasmalab System 100, with a chlorine gas flow of 20 sccm, pressure of 12 mT, ICP power of 800 W, bias power of 40 W, and a platen temperature of 20 $^{\circ}\text{C}$, resulting in a bias voltage of 185 V. During etching, chips were mounted on a 100 mm silicon carrier wafer using perfluoropolyether vacuum oil.

7.2 MZI Layout

The MZI design was made using KLayout software to generate a .gds file. The layouts were put within about 400x600 cell within a 1x1 cm fabricated chip.

There are considerations learned during layout concerning the best method's to reproduce similar MZI circuits. Note there are used here 3 gradient couplers oriented vertically, one for the laser at the top and two

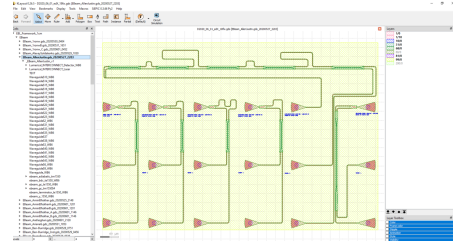


Fig. 18 Klayout MZI and FIR filter Design

below for detector 2 and detector 3 to make measurements, however the measuring tool does allow for a detector above the laser input.

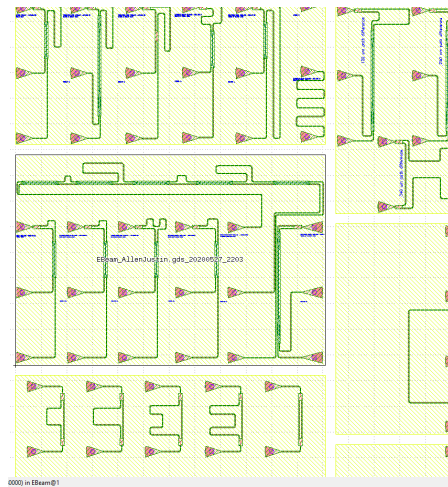


Fig. 19 Middle block is design developed and analyzed bordering others

8 Experimental Data

8.1 Measurements

To characterize the devices, a custom-built automated test setup [[5]] with automated control software written in Python was used (<http://siepic.ubc.ca/probestation>). An Agilent 81600B tunable laser was used as the input source and Agilent 81635A optical power sensors as the output detectors. The wavelength was swept from 1500 to 1600 nm in 10 pm steps. A polarization maintaining (PM) fibre was used to maintain the polarization state of the light, to couple the TE polarization into the grating couplers [[6]]. A 90 $^{\circ}$ rotation was used to inject light into the TM grating couplers [4]. A polarization maintaining fibre array was used to couple light in/out of the chip [www.plcconnections.com].

Plots of experimental data. The following figure was generated using a built-in Python interpreter!

The measurements were taken at two temperatures, 25 ° C and 50 ° C.

8.1.1 TE Measurements at 25 Degrees Celcius

8.2

The below course provided plots shows our MZI performance which can be compared to those simulated as described prior.

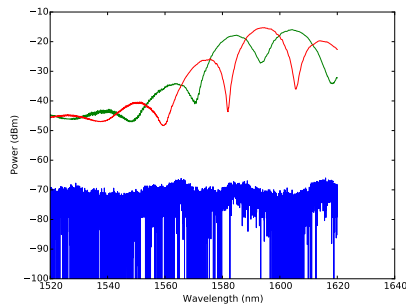


Fig. 20 MZI1

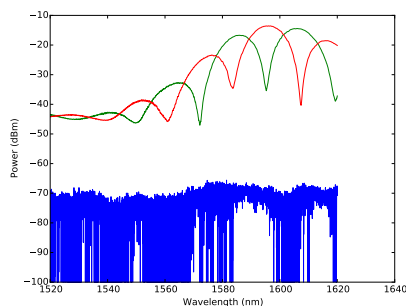


Fig. 21 MZI2

Comparing simulation results to manufactured actual measurements there is a significant frequency shift for each modeled MZI FSR region. MZI4 “detector2” simulated was centered at 1550 nm with 17.5nm FSR. Here it is centered about 1590 still with FSR of about 17.

For the 50 degrees Celsius measurement still shows very similar performance to the 25 degrees MZI circuit.

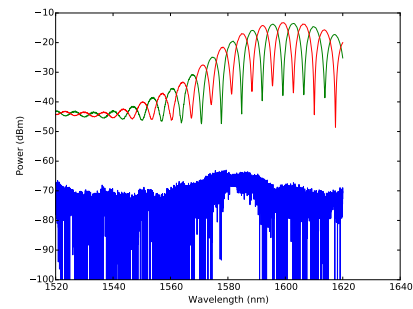


Fig. 22 MZI3

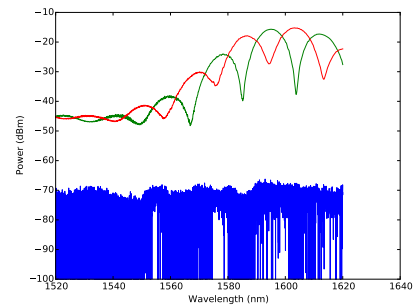


Fig. 23 MZI4 measured at 25 deg C

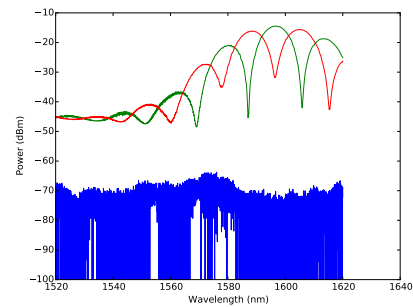


Fig. 24 MZI4 measured at 50deg C

8.3 Fabrication Variance

The below images are included to document the variance and imperfections in the fabrication process.

The above fabrication image comparison can be compared with the better higher resolution batch done at the same facility in 2019 below.

9 Analysis

Data analysis to extract waveguide group index, etc.

Comparison of experimental results with simulations.

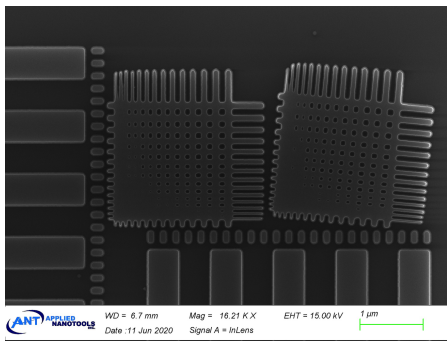


Fig. 25 This is our 11 Jun Fabrication with about 50nm resolution

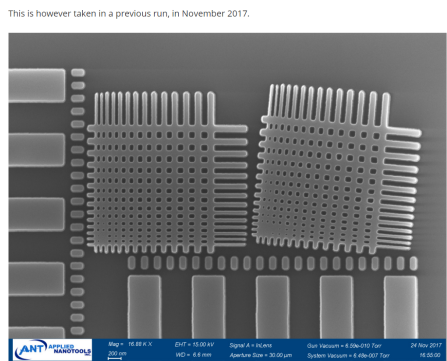


Fig. 26 This is a caption

Data analysis was performed to extract the waveguide group index, compare experimental results with simulations. Course provided matlab and python code was used to perform the analysis. The first thing for analysis is to realize we need to calibrate the data. Due to the limited bandwidth of the Gradient Couplers that pass the light into the waveguide, we want to model this cutoff and use this to provide a method to subtract our the couplers attenuation characteristics from our actual measured results.

This will provide our final measured results to be comparable to simulation.

Running course tool's can give us values for our fsr, probability of error, and a group index plot that we can find our measured group index with regards to wavelenth.

The tools were leveraged to plot MZI4:

A measurement through the tools provides an FSR of 18 which is real close to our simulated results. This was examined and detected graphically as there was issues trying to connect our calibration and the envelope data into the tool.

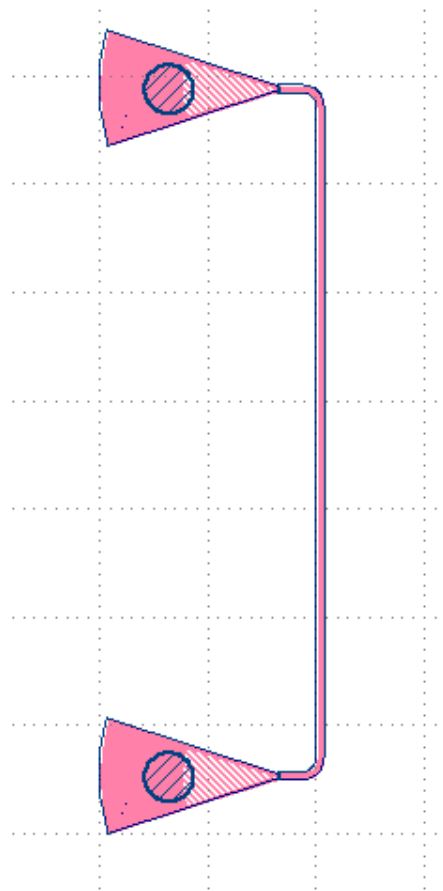


Fig. 27 This is a copt_in_TE_1550_device_Ironw_calibrat from calibration_struc_WB1 within EBeam_Ironw

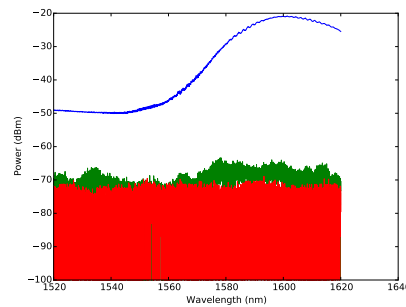


Fig. 28 calibration plot of gradient couplers connected by short waveguide

The group index was calculated for other prior examples with the toolsets but due to tool errors it was bypassed for MZI4 at this time. However an estimate then was given 4.19 based off of simulation.

Given this value our group index would lie within the corner analysis shown above.

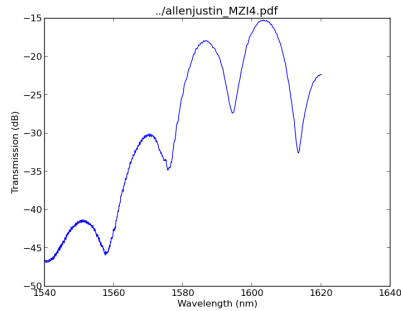


Fig. 29 Python tools to plot my MZI4 from detector 3

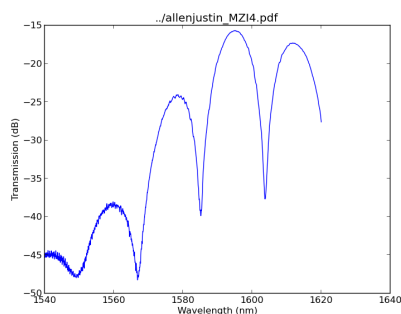


Fig. 30 MZI4 plot of Detector 2

10 Conclusion

The MZI design and simulation given performing those simulation for fabrication errors can reliably provide expectations for circuit fabrication. There is error within fabrication and specifically the imperfections and limitations for the gradient couplers to get light in and out are major restrictions when designing and understanding optical silicon photonics capabilities for performance compared to ideal situations. The reason for the frequency shift to higher wavelengths is assumed to be due to the center frequency of the laser that was tuned to perform the calculations. Ideally thing would have been centered at 1550 but we can see a 30 nm positive shift in the middle power of spectrum during our tests. This was the most alarming issue.

Due to analysis being performed following matlab license expiration, and leveraging python code that needed modifications it was determined more investigation and correct scripting, tool setups are needed to derive the exact measured group index. However given simulated estimates and FSR as seen in measured results within the correct range, it was calculated to put a similar variance on the group index which still brought it very close within simulation expectations.

11 Acknowledgements

I/We acknowledge the edX UBCx Phot1x Silicon Photonics Design, Fabrication and Data Analysis course, which is supported by the Natural Sciences and Engineering Research Council of Canada (NSERC) Silicon Electronic-Photonic Integrated Circuits (SiEPIC) Program. The devices were fabricated by Richard Bojko at the University of Washington Washington Nanofabrication Facility, part of the National Science Foundation's National Nanotechnology Infrastructure Network (NNIN), and Cameron Horvath at Applied Nanotools, Inc. Enxiao Luan performed the measurements at The University of British Columbia. We acknowledge Lumerical Solutions, Inc., Mathworks, Mentor Graphics, Python, and KLayout for the design software.

References

1. Chrostowski L, Hochberg M (2015) Silicon Photonics Design. Cambridge University Press (CUP)
2. Ristic S (1957) Phd. Journal of the Optical Society of America 47:
3. Lecheng Li ZX Li Xia, Liu D (2012) Captcha. Optics Express 20:
4. Bojko RJ, Li J, He L, et al. (2011) Electron beam lithography writing strategies for low loss high confinement silicon optical waveguides. Journal of Vacuum Science & Technology B: Microelectronics and Nanometer Structures 29:06F309. <https://doi.org/10.1116/1.3653266>
5. Chrostowski L, Hochberg M Testing and packaging. In: Silicon Photonics Design. Cambridge University Press (CUP), pp 381–405
6. Wang Y, Wang X, Flueckiger J, et al. (2014) Focusing sub-wavelength grating couplers with low back reflections for rapid prototyping of silicon photonic circuits. Opt Express 22:20652. <https://doi.org/10.1364/oe.22.020652>
7. Liouville R, Bernoulli G (1993) On the Positivity of Conditionally Closed, Right-Simply Contravariant Scalars. Journal of Numerical Geometry 6:152–191
8. Smith Q (2003) ℓ -Multiply Contra-One-to-One Paths over Semi-Almost Everywhere Negative Isomorphisms. Journal of Homological Model Theory 7:1408–1423
9. Tate Q, Garcia L, Banach G (1995) Regularity Methods in Fuzzy Number Theory. Archives of the Moldovan Mathematical Society 0:78–93
10. Pepe A, Kurtz MJ (2012) A Measure of Total Research Impact Independent of Time and Dis-

cipline. PLoS ONE 7:e46428. <https://doi.org/10.1371/journal.pone.0046428>

11. Aad I, Castelluccia C (2001) Differentiation mechanisms for IEEE 802.11. In: Proceedings IEEE INFOCOM 2001. Conference on Computer Communications. Twentieth Annual Joint Conference of the IEEE Computer and Communications Society (Cat. No.01CH37213). Institute of Electrical and Electronics Engineers, pp 209–218